Coherent Kinks in High-Power Ridge Waveguide Laser Diodes

Martin Achtenhagen, Amos A. Hardy, *Fellow, IEEE*, *Fellow, OSA*, and Christoph S. Harder, *Member, IEEE*

***Abstract*—Coherent coupling of lateral modes is suggested to explain the phenomena associated with beam-steering kinks, which appear in the $L-I$ curves of many ridge waveguide lasers. The analysis that is presented explains quantitatively the previously reported experiments.**

***Index Terms*—Laser modes, modeling, semiconductor device modeling, semiconductor lasers.**

I. Introduction

In recent years, high-power ridge waveguide (RWG) laser diodes at $\lambda = 980$ nm have been widely used in a variety of applications such as pump sources in Er-doped fiber amplifiers (EDFAs). These lasers are renowned for their reliability, beam quality, and high power output [1], [2]. Present-day applications, however, are limited by the maximum kink-free power output available from these devices.

Experimental results presented in the literature [3]–[7] produced $L-I$ curves for RWG lasers of the type shown in Fig. 1. At the so-called "kink," there is a slight beam steering [4], [8]–[11] on the order of 1°–3°, which can cause a significant reduction of the power available for coupling into a single-mode fiber. Observations of the spontaneous emission, from the top of the device, showed a beat pattern along the laser ridge [9], [10]. When the $L-I$ curve measurements are made with short ($<$ 100 ns) pulses and with a low duty cycle, the coherent kinks are shifted to higher power levels [12], [13], indicating that indeed a temperature rise is involved.

The most common explanation for kinks is that the laser oscillates simultaneously in the two lowest order lateral modes (TE_0 and TE_1 at ν_0 and ν_1), which are both above threshold [9], [14], [15]. This explanation, however, fails to describe the observed beam steering as well as the beat pattern in the top-side spontaneous emission. A model that assumes that the two modes are locked in frequency and phase, on the other hand, explains the beam-steering kink and mode-beating phenomena. Since the two modes oscillate at a common frequency ν, we shall refer to these kinks also as coherent kinks to distinguish them from ordinary kinks [16], [17].

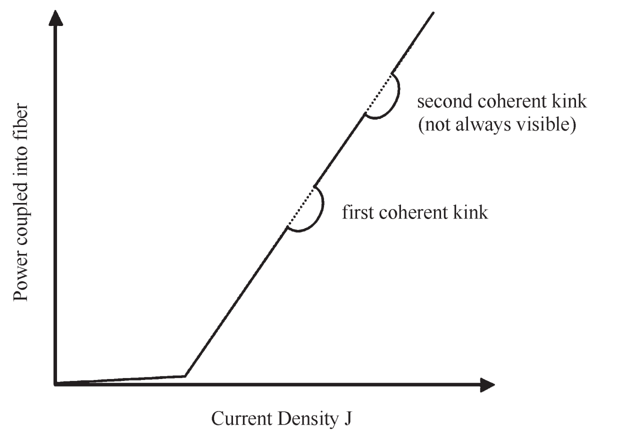

Fig. 1. Typical $L-I$ curve for high-power RWG lasers. Kinks are observed when a limited aperture detector is used or when the light coupled into a fiber is measured. Usually, only one kink is observed.

To illustrate the proposed mechanism, let us consider the RWG drawn schematically in Fig. 2(a). Employing the effective-index method, we obtain an effective lateral waveguide, the refractive-index distribution of which is shown in Fig. 2(b). Calculating the propagation constant for the two lowest order lateral modes, namely, TE_0 and TE_1, as a function of frequency ν or free space wavenumber $k_0 = 2\pi\nu/c_0$, we obtain the schematic dispersion diagram depicted in Fig. 2(c).

A laser mode, oscillating at frequency ν and having a propagation constant β, must satisfy the resonance condition $2L\beta = 2\pi q$, where L is the laser length, and q is an integer. In the dispersion diagram of Fig. 2(c), we note that the TE_0 mode satisfies the resonance condition at some point "A" with frequency ν_0, whereas the TE_1 mode satisfies the resonance condition at some other point "B" at frequency ν_1 (where $p \neq q$ are both integers). This is the usual situation, i.e., the two modes oscillate simultaneously at two different frequencies $\nu_0 \neq \nu_1$, as can be verified experimentally by measuring their beat frequency $\Delta\nu = \nu_0 - \nu_1$. Only accidentally, the TE_1 mode can oscillate exactly at the point "C" with frequency $\nu_1 = \nu_0$. Thus, most often, one may expect that due to spatial-hole burning, two or more modes will reach threshold and oscillate simultaneously at different frequencies, thereby creating ordinary incoherent kinks. Nevertheless, from the experimental evidence in the literature, one finds that many RWG lasers (not just a few) show the beam-steering-kink phenomena (i.e., lasing in two coherent lateral modes that are locked in frequency and

Manuscript received November 9, 2005; revised February 6, 2006. The work of A. A. Hardy was supported by the Chana and Heinrich Manderman Chair in Optoelectronics at Tel-Aviv University.

M. Achtenhagen is with the Laboratory of Physics of Nanostructures, Ecole Polytechnique Fédérale de Lausanne, Lausanne 1015, Switzerland, and also with IBM, Ruschlikon, Switzerland (e-mail: martin.achtenhagen@epfl.ch).
A. A. Hardy is with the Laboratory of Physics of Nanostructures, Ecole Polytechnique Fédérale de Lausanne, Lausanne 1015, Switzerland, and also with the Department of Electrical Engineering–Physical Electronics, Tel-Aviv University, Tel-Aviv 69978, Israel (e-mail: hardy@eng.tau.ac.il).
C. S. Harder is with the Swiss Federal Institute of Technology, Zurich 8092, Switzerland.

Digital Object Identifier 10.1109/JLT.2006.872313

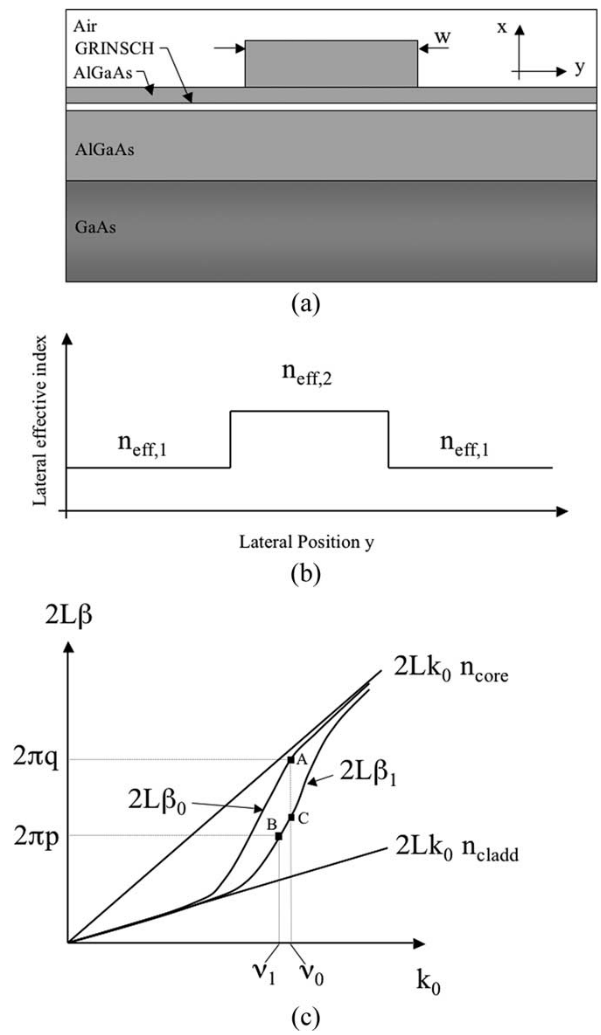

Fig. 2. Typical RWG laser. (a) Cross-sectional diagram. (b) Corresponding lateral effective-index distribution. (c) Schematic of the dispersion diagram, for the three-layer symmetric slab waveguide of (b), as a function of the free-space wavenumber k_0. The ordinate is in units of $2L\beta$ to indicate the laser resonances for each mode.

phase). In addition, a similar phenomenon has been found in vertical-cavity surface-emitting laser structures [18].

Furthermore, as the current density is gradually increased, the laser goes through several phases. Initially, above threshold, the $L-I$ curve is linear, and the laser oscillates in a single lateral mode (the TE_0 mode). Then, at some specific power level, the first coherent kink is observed, presumably due to the onset of the TE_1 mode, which has reached threshold. With a further increase in the injected current density, the coherent kink disappears, and the RWG laser oscillates again in a single mode. As the current density is still further increased, quite often, a second coherent kink is observed [7], [12] and later, for higher current densities, disappears. It is quite difficult to explain how the TE_1 mode could stop and start oscillating time and again once it reached threshold at some lower current densities.

From the experimental observations, we conclude that if coherent kinks are created, as opposed to the incoherent ones, the TE_1 mode must still be below threshold. Rather, it is driven and constantly fed by the oscillating fundamental mode. The mechanism for this effect is an elastic scattering (i.e., same wavelength) of light from the oscillating TE_0 mode into the below-threshold TE_1 mode by means of any type of asymmetrically distributed imperfections and defects (e.g., hot spots, scratches, tilted mirrors, Rayleigh scattering, etc.). That is, the fundamental mode constantly feeds the TE_1 mode, at the same wavelength, whether or not the latter mode is in resonance. Due to reciprocity, a similar scattering occurs from the TE_1 mode into the TE_0 mode. It is emphasized here that this scattering should be an elastic process. Otherwise, light scattered from the oscillating TE_0 mode at point "A" could feed the TE_1 mode at point "B," which resonates at a different frequency. Even if the latter mode is not above threshold, this should result in an incoherent kink.

It is clear that as long as the driven TE_1 mode at point "C" is not in resonance, it will remain negligibly small due to destructive interference. As the current density increases, the junction temperature underneath the ridge also rises, resulting in an increased effective-index step $(\partial n/\partial T > 0)$ and increased $\Delta\beta = \beta_0 - \beta_1$. Eventually the TE_1 mode gets into resonance. If elastic scattering into the TE_1 mode is strong enough to overcome the extra cavity losses, the TE_1 mode builds up on the account of the driving TE_0 mode and a coherent kink is generated. With a continued increase of the current density, the temperature difference ΔT is further elevated, and the driven TE_1 mode gets out of resonance again.

In the next section, the mathematical equations for this phenomenon are presented, along with vital remarks regarding their solution method. Some numerical examples and discussions are given in Section III. Finally, concluding remarks are given in Section IV.

II. Mathematical Model

Although the following model can be adapted to any index-guided semiconductor laser, for definiteness, we consider a weakly index-guided single quantum-well (QW) InGaAs laser. The objective is to obtain the steady-state device characteristics under the influence of coherent lateral-mode coupling. Therefore, we derive a set of phenomenological equations, in which we include coupling terms. The equations are solved in a self-consistent manner with the effect of nonlinear gain distribution due to the stimulated recombination.

The electric-field distribution in the cavity is represented as a superposition of forward- and backward-propagating modes, namely

$$E(y,z) = \sum_{p=0}^{1} \left[E_p^{+}(z) + E_p^{-}(z)\right] \cdot G_p(y) \tag{1}$$

where $G_p(y)$, $p = 0{,}1$ are the lateral-mode profiles of the quasi-TE_0 and TE_1 modes, respectively, for the effective waveguide of Fig. 2(b). As a matter of convenience, these modes are normalized to satisfy

$$\int_{-\infty}^{\infty} G_p(y) \cdot G_q(y) \cdot dy = Q_p \cdot \delta_{pq} \tag{2}$$

where Q_p, $p = 0,1$ is the effective width in which the mode TE_p is concentrated, and δ_{pq} is the Kronecker delta function, which equals unity for $p = q$, and zero otherwise. The field coefficients $E_p^{\pm}(z)$ then satisfy a set of four coupled equations

$$\pm\frac{dE_p^{\pm}(z)}{dz} = \left[i\beta_p + \frac{1}{2}\left(\Gamma_p g(z) - \alpha\right)\right]\cdot E_p^{\pm}(z) + i\kappa(z)\cdot E_q^{\pm}(z)$$
$$p = 0,1, \quad q = 0,1, \quad p \neq q \quad (3)$$

in which β_0 and β_1 are the two propagation constants at the same wavelength λ, $g(z)$ is the local material gain per unit length, α is the scattering loss per unit length, Γ_p is the power filling factor in the active region ($\Gamma_p = \Gamma^x \Gamma_p^y$), and $\kappa(z)$ is a coupling coefficient expressed by

$$\kappa(z) \propto \int_{-\infty}^{\infty} \Delta n^2(y,z)\cdot G_0(y)\cdot G_1(y)\cdot dy \quad (4)$$

where $\Delta n^2(y,z)$ is the index perturbation. Note that only asymmetrical perturbations may couple the two lowest order lateral modes. In the present analysis, we select some arbitrary numerical values for $\kappa(z)$. Furthermore, in this simple model, the lateral power filling factors Γ_p^y are constants and not affected by current spreading, carrier diffusion, or spatial-hole burning.

In order to eliminate rapid phase variations, we define

$$E_p^{+}(z) = A_p\cdot\exp(i\beta_p z), \qquad p = 0,1 \quad (5a)$$
$$E_p^{-}(z) = B_p\cdot\exp(-i\beta_p z), \qquad p = 0,1 \quad (5b)$$

and (3) reduce to

$$\frac{d}{dz}U = M\cdot U \quad (6a)$$

where the transpose of U is $U^{\mathrm{T}} = (A_0, B_0, A_1, B_1)$, and M is given by (6b), shown at the bottom of the page. Note the phase terms in (6b). Since the field propagating in the cavity sees the same conditions every round trip, the coupling coefficient has a natural period of $2L$, and the main contribution to the mode coupling comes from the Fourier component that approximately cancels the phase term. This is exactly the source of our coherent kinks. It is implicitly assumed that the TE_0 mode is in resonance and oscillates at any current density above threshold. Thus, unless the resonance condition $2L\Delta\beta = 2\pi m$ is approximately met, there is no Fourier component of $\kappa(z)$ that cancels the phase terms in (6b), and therefore, the coupling of the oscillating TE_0 mode into the driven TE_1 mode will average out to zero. Note also that (6a) and (6b) resembles the coupled-mode equations of Kogelnik [19], except that the self-coupling terms include the local z-dependent saturable material gain per unit length $g(z)$, where [20]

$$g(z) = g_0\cdot\ln\left(\frac{N(z)}{N_{\mathrm{tr}}}\right). \quad (7)$$

In (7), $N(z)$ is the injected carrier density, N_{tr} is the carrier density necessary to reach transparency, and g_0 is a constant. The numerical values of N_{tr} and g_0, as well as other parameters, are given in Table I. The carrier density $N(z)$ and its dependence on the photon density is given by

$$\frac{\eta_{\mathrm{i}}\cdot J}{q\cdot d} = \frac{N}{\tau(N)} + g(N)\left(\frac{1}{\hbar\omega}\cdot\frac{n_{\mathrm{eff}}}{2c_0\mu}\right)$$
$$\times\left(|A_0|^2 + |B_0|^2 + |A_1|^2 + |B_1|^2\right) \quad (8)$$

where q is the elementary charge, d is the QW thickness, J is the current density per unit area, η_{i} is the internal quantum efficiency, c_0 is the speed of light in free space, μ is the permeability, and $\tau = (a + bN + cN^2)^{-1}$ is the spontaneous carrier lifetime, which includes radiative- and nonradiative-recombination as well as Auger-recombination terms. The numerical values of these parameters are given in Table I. Interference terms between A_0 and A_1, as well as between B_0 and B_1, do not appear on the right-hand side of (8), because of the orthogonality relation (2). Also, the interference between forward- and backward-propagating modes is washed out by axial carrier diffusion and does not appear in (8). As mentioned above, the effects of lateral carrier diffusion and current spreading are neglected in the present simplified analysis.

Assuming a back mirror at $z = -L/2$, with power reflectivity, for the TE_0 and TE_1 modes, of $R_{\mathrm{b},p}$, $p = 0,1$, respectively, and a front mirror (from which power is extracted) at $z = L/2$, with power reflectivity of $R_{\mathrm{f},p}$, the boundary conditions are

$$E_p^{+}(-L/2) = \sqrt{R_{\mathrm{b},p}}\cdot E_p^{-}(-L/2), \quad p = 0,1 \quad (9a)$$
$$E_p^{-}(L/2) = \sqrt{R_{\mathrm{f},p}}\cdot E_p^{+}(L/2), \qquad p = 0,1 \quad (9b)$$

or, in terms of the slowly varying envelope functions A_p and B_p, we obtain

$$A_p(-L/2) = \sqrt{R_{\mathrm{b},p}}\cdot B_p(-L/2)\cdot\exp\left(i\cdot\beta_p\cdot L\right) \quad (10a)$$
$$B_p(L/2) = \sqrt{R_{\mathrm{f},p}}\cdot A_p(L/2)\cdot\exp\left(i\cdot\beta_p\cdot L\right). \quad (10b)$$

$$M = \begin{pmatrix} \frac{1}{2}(\Gamma_0 g - \alpha) & 0 & i\kappa(z)\cdot e^{-i\cdot\Delta\beta\cdot z} & 0 \\ 0 & -\frac{1}{2}(\Gamma_0 g - \alpha) & 0 & -i\kappa(z)\cdot e^{i\cdot\Delta\beta\cdot z} \\ i\kappa(z)\cdot e^{i\cdot\Delta\beta\cdot z} & 0 & \frac{1}{2}(\Gamma_1 g - \alpha) & 0 \\ 0 & -i\kappa(z)\cdot e^{-i\cdot\Delta\beta\cdot z} & 0 & -\frac{1}{2}(\Gamma_1 g - \alpha) \end{pmatrix} \quad (6b)$$

TABLE I
LIST OF THE MATERIAL AND RWG LASER PARAMETERS

Parameter description	Symbol	Value
Radiation wavelength	λ	0.98 μm
Laser length	L	750 μm
Ridge width	w	4.0 μm
QW thickness	d	80 Å
Front facet reflectivity for TE_0 power	$R_{f,0}$	0.1
Back facet reflectivity for TE_0 power	$R_{b,0}$	0.9
Front facet reflectivity for TE_1 power	$R_{f,1}$	0.09
Back facet reflectivity for TE_1 power	$R_{b,1}$	0.89
Non-radiative recombination coefficient	a	2.1×10^{8} s^{-1}
Spontaneous radiative recombination term	b	8×10^{-11} cm^3s^{-1}
Auger coefficient	c	3.5×10^{-30} cm^6s^{-1}
Scattering loss	α	5 cm^{-1}
Transparency carrier density	N_{tr}	1.8×10^{18} cm^{-3}
Gain constant	g_0	2400 cm^{-1}
Transversal power filling factor	Γ^x	0.015
Lateral power filling factor for TE_0	Γ_0^y	0.90
Lateral power filling factor for TE_1	Γ_1^y	0.87
Internal efficiency	η_i	0.9

Thus, in addition to the slow phase change of $A_p(z)$ and $B_p(z)$ along the laser, they also accumulate a phase difference of $\exp(i2\beta_p L)$ each complete cavity round trip. Finally, the near-field distribution just outside the front mirror is given by

$$E_{\text{out}}(y) = \sqrt{1-R_{\text{f},0}} \cdot E_0^+(L/2) \cdot G_0(y) + \sqrt{1-R_{\text{f},1}} \cdot E_1^+(L/2) \cdot G_1(y). \quad (11)$$

The far-field distribution of the output field is given by the Fourier transform of $E_{\text{out}}(y)$ [21]. The total power output is obtained by integrating over the power density (the Poynting vector's z-component), which, due to the orthogonality relation (2), results in

$$P_{\text{out}} = \left(\frac{Q\cdot n_{\text{eff}}}{2\cdot c_0\cdot \mu}\right) \Big\{(1-R_{\text{f},0})\cdot|A_0(L/2)|^2 + (1-R_{\text{f},1})\cdot|A_1(L/2)|^2\Big\} \quad (12)$$

where $Q_0 \approx Q_1 = Q$ was used. As we shall see in the next section, the total power output increases linearly with pumping current density, whether or not the TE_1 mode is excited. However, the power coupled into a single-mode fiber, will show the coherent-kink nonlinearities, due to the beam steering, and is obtained directly from the far-field distribution.

III. Discussion and Results

We apply our model to the laser structure shown in Fig. 2, including some simplified thermal considerations (i.e., a temperature rise of ΔT only underneath the ridge). From a spectral shift measurement [22], we find the approximate temperature rise, as a function of the current density. Assuming $\partial n/\partial T = 3\times10^{-4}$, one obtains a monotonic increase of $\Delta\beta$ with current density (see Fig. 3). As a matter of convenience, we plot the resonance difference $2L\Delta\beta/2\pi$. That is, we keep the TE_0 mode at a cavity resonance of $2L\beta_0 = 2\pi q$ (implicitly assuming a gradual wavelength shift with the increase of Δn_{eff}), and when

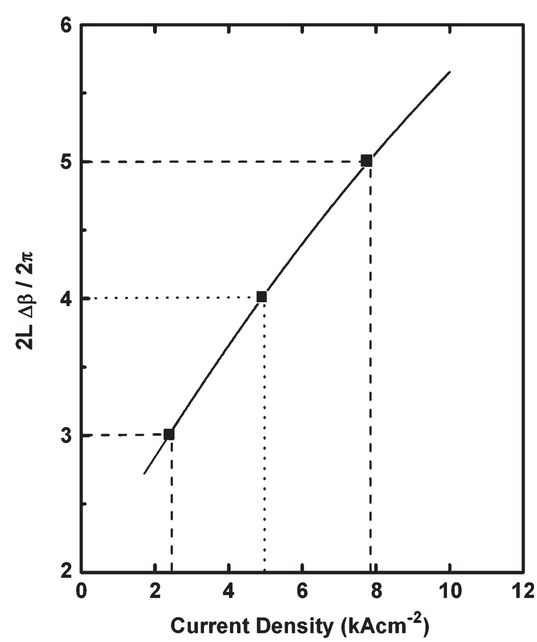

Fig. 3. Variation of $\Delta\beta = \beta_0 - \beta_1$ with the injected current density. Indicated are the conditions for the coherent-kink resonances. For current densities smaller than 1.8 kA/cm^2, the TE_1 mode is cut off. The temperature rise ΔT at m = 3, 4, and 5 amounts to 9.5, 15, and 23 °C, respectively.

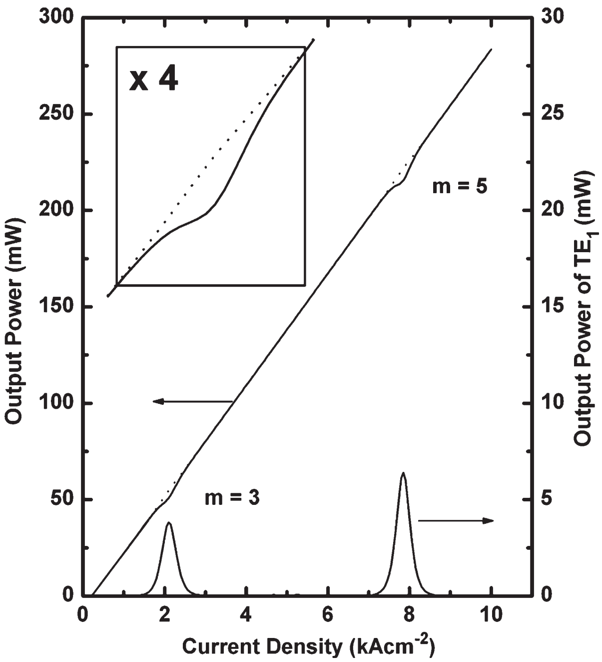

Fig. 4. Power output as a function of current density. The total power is nearly linear above threshold. At the location of the coherent kinks, there is a significant contribution from the TE_1 mode. The inset shows a fourfold magnification of the $m = 5$ resonance.

the TE_1 cavity resonance of $2L\beta_1 = 2\pi p$ is reached, we define the coherent-kink order m as

$$m \equiv q - p = 2L\Delta\beta/2\pi. \tag{13}$$

Note that, for our specific example, the $m = 3$ coherent kink is just barely above cutoff.

The power output as a function of the injected current density is depicted in Fig. 4. The solid lines represent the power in the TE_0 and TE_1 modes separately. However, when a totally integrating sphere is used to measure the power output, the total power in both modes is detected, which is described by the dotted lines. The coherent kinks are actually obtained only when a limiting aperture (e.g., single-mode fiber) is used. The inset shows a four-times magnification of the $m = 5$ resonance and its vicinity. Note the missing of the $m = 4$ resonance. Here, and in the examples that follow, the coupling coefficient was arbitrary selected as

$$\kappa(z) = \begin{cases} 2\ \mathrm{cm}^{-1}, & -\frac{L}{2} \le z < 0 \\ -2\ \mathrm{cm}^{-1}, & 0 \le z \le \frac{L}{2} \end{cases}. \tag{14}$$

Since the even-order Fourier components of $\kappa(z)$ vanish, the $m = 4$ resonance does not appear. Although the fifth-order Fourier component of $\kappa(z)$ is smaller than the third-order Fourier component, nevertheless, the $m = 5$ resonance contains more power due to the higher injected current.

The power density $|E(y,z)|^2$ along the cavity for the $m = 3$ resonance is presented in Fig. 5. There are exactly three maxima alternatively shifted from the optical axis, which originate from the lateral-mode beating, in agreement with previously reported experimental measurements [9], [10]. The power density at the front mirror is higher than that near the back mirror due to the higher reflectivity of the latter. Similarly, the power density for the $m = 5$ resonance is drawn in Fig. 6. Here, we have five maxima, which are alternatively shifted from the optical axis. Since the injected current density is significantly higher than at the $m = 3$ resonance, the power density is also much higher, resulting in a slightly more pronounced internal power asymmetry.

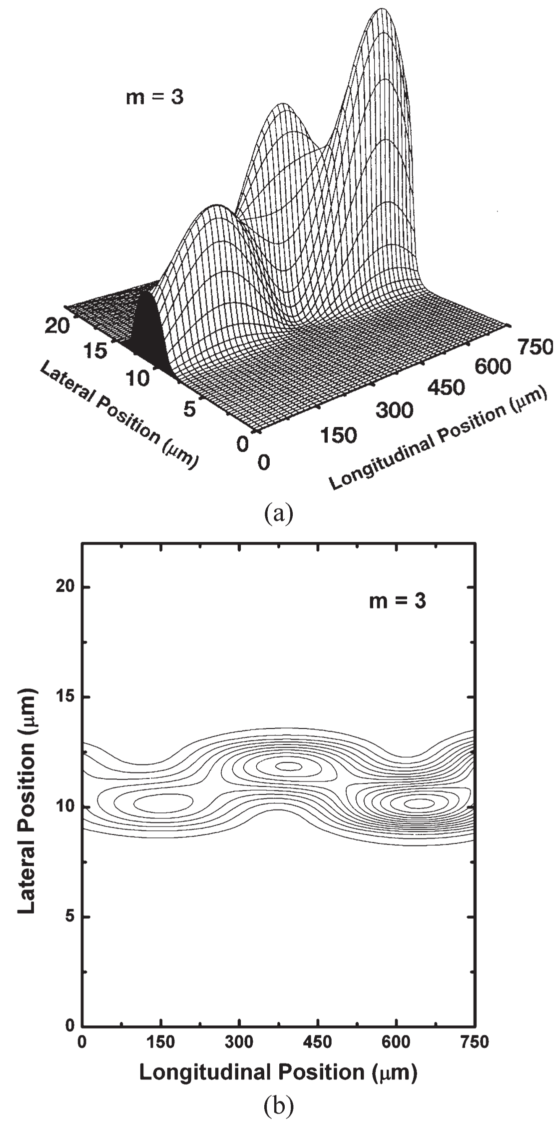

Fig. 5. Lateral and longitudinal intensity distribution inside the laser cavity for the $m = 3$ resonance. (a) Three-dimensional plot of the energy density. (b) Contour diagram of the energy distribution.

The far-field distribution of the output field at the $m = 5$ resonance is given in Fig. 7 (solid line). For comparison, the far-field pattern of the TE_0 mode (dashed line) is also presented. Note the significant steering of the combined mode, which amounts to a 3° beam shift. Statistically, 50% of the lasers may have index perturbations $\Delta n^2(y,z)$ located on one side of the optical axis, whereas the other lasers may have the index perturbations located on the opposite side. Therefore, the

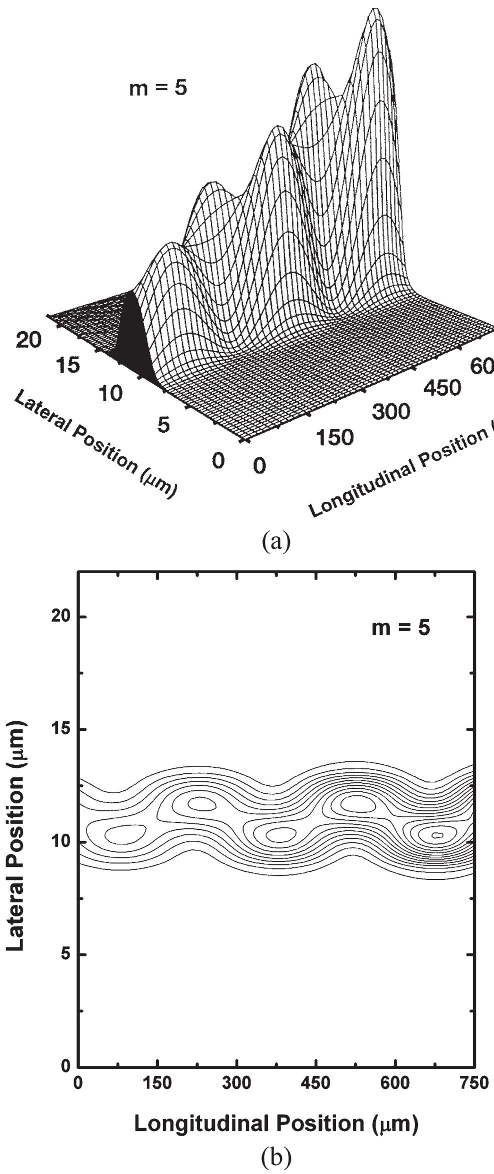

Fig. 6. Lateral and longitudinal intensity distribution inside the laser cavity for the $m = 5$ resonance. (a) Three-dimensional plot of the energy density. (b) Contour diagram of the energy distribution.

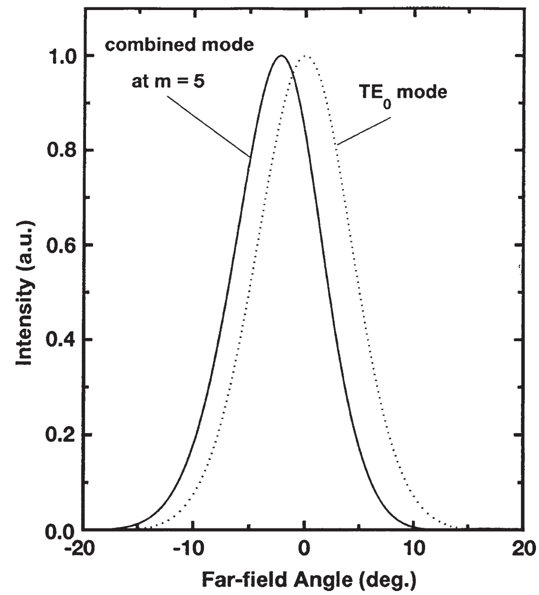

Fig. 7. Far-field pattern of the combined field (TE_0 and TE_1) at the coherent kink of order $m = 5$ (solid line). The far-field distribution of the TE_0 mode (dotted line) is given as a reference.

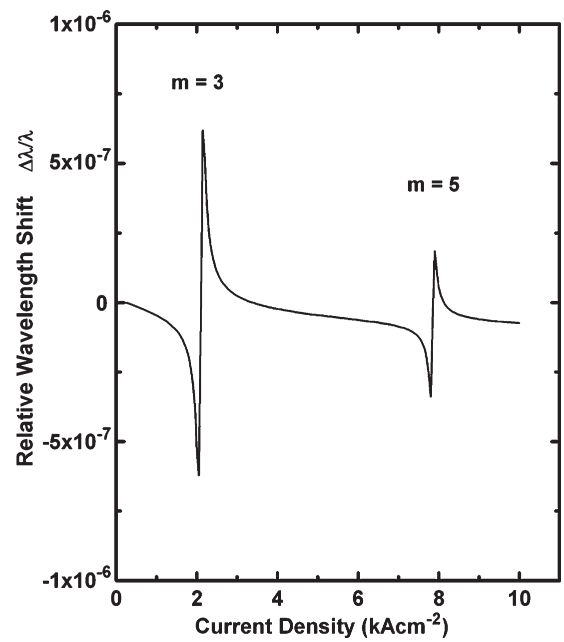

Fig. 8. Relative wavelength shift as a function of current density due to the coherent coupling between the TE_0 and TE_1 modes.

sign of the coupling coefficient $\kappa(z)$ [see (4)] will differ for the two groups. As a result, half of the lasers will have their output beam shifted to the opposite direction. It is worthwhile to indicate that the amount of beam steering is a monotonic function of the coupling-coefficient magnitude.

The far-field pattern determines the amount of light coupled into a fiber. This is because the fiber core does not trap angular spectrum components that propagate at angles larger than the numerical aperture of the fiber. The amount of power coupled into a fiber is an important parameter that determines the power in the coherent kinks. For a typical direct-coupled single-mode fiber, only the TE_0 mode couples, and thus, with numerical aperture of 0.11, the power coupled into the fiber core is reduced by nearly 5% (experimentally measured) at the $m = 5$ resonance. Therefore, one obtains an $L-I$ curve similar to Fig. 4.

We note that at, and near, the coherent kinks, the power contained in the TE_1 mode may be quite significant to influence the oscillating lowest order TE_0 mode. Since the coupling term in (3), which includes the TE_1-mode amplitude, is complex, the phase of the fundamental mode will also be affected. Therefore, the wavelength at which the lasing TE_0 mode oscillates is significantly shifted near each of the coherent kinks. In Fig. 8, we present the relative wavelength shift $\Delta\lambda/\lambda$, from the oscillating wavelength at threshold λ_{th}, as a function of the injected current density, where $\Delta\lambda = \lambda - \lambda_{\text{th}}$. Note that this shift is solely due to the coupling effect. It does not include band-gap change with temperature and the direct impact of the index variation with temperature. Therefore, the wavelength shift, which clearly demonstrates a resonance phenomenon, vanishes at the center of each of the coherent kinks.

IV. CONCLUSION

In this paper, a simple model has been presented in order to explain beam-steering kinks in the $L-I$ curve of RWG lasers. It is postulated that the source of these kinks is an elastic coupling between the oscillating TE_0 mode, which is above threshold, and a driven TE_1 mode, which is below threshold due to its excess mirror losses and/or smaller power filling factor. As the injected current density is increased, and with it the junction temperature, the TE_1 mode is brought in and out of resonance time and again, drawing power from the TE_0 mode at each coherent kink. In this model, the physical mechanism for the mode coupling could be any asymmetric perturbation, which is lumped into a coupling parameter. That is, two different perturbations (e.g., a scratch or a hot spot), at different locations, may cause the same coherent kinks, as long as the appropriate Fourier components of the coupling coefficients are the same. It is shown that the coupled differential equations, which include saturable gain, give rise to all the phenomena reported earlier in association with the coherent kinks. In this paper, various lateral effects, such as current spreading, carrier diffusion, and lateral spatial-hole burning, were neglected. These may affect the magnitude of the coherent-kink phenomenon and will be considered elsewhere.

REFERENCES

[1] A. Oosenbrug and A. Jakubowicz, "Operational stability of 980-nm pump lasers at 200 mW and above," *Proc. SPIE*, vol. 3004, pp. 62–70, 1997.

[2] N. Chand, S. N. G. Chu, N. K. Dutta, J. Lopata, M. Geva, A. V. Syrbu, A. Z. Mereutza, and V. P. Yakovlev, "Growth and fabrication of high-performance 980-nm strained InGaAs quantum-well lasers for Erbium-doped fiber amplifiers," *IEEE J. Quantum Electron.*, vol. 30, no. 2, pp. 424–439, Feb. 1994.

[3] C. Harder, P. Buchmann, and H. Meier, "High-power ridge-waveguide AlGaAs GRIN-SCH laser diode," *Electron. Lett.*, vol. 22, no. 20, pp. 1081–1082, Sep. 1986.

[4] J. Näppi, A. Ovtchinnikov, H. Asonen, P. Savolainen, and M. Pessa, "Limitations of two-dimensional passive waveguide model for $\lambda = 980$ nm Al-free ridge waveguide lasers," *Appl. Phys. Lett.*, vol. 64, no. 17, pp. 2203–2205, Apr. 1994.

[5] J. Temmyo and M. Shimizu, "Strained InGaAs quantum well lasers with small-divergence angles for high-power pump modules," *Electron. Lett.*, vol. 30, no. 24, pp. 2046–2047, Nov. 1994.

[6] J. Temmyo and M. Sugo, "Design of high-power strained InGaAs/AlGaAs quantum-well lasers with a vertical divergence angle of 18°," *Electron. Lett.*, vol. 31, no. 8, pp. 642–644, Apr. 1995.

[7] P. Savolainen, M. Toivonen, H. Asonen, M. Pessa, and R. Murison, "High-performance 980-nm strained-layer GaInAs–GaInAsP–GaInP quantum-well lasers grown by all solid-source molecular-beam epitaxy," *IEEE Photon. Technol. Lett.*, vol. 8, no. 8, pp. 986–988, Aug. 1996.

[8] M. F. C. Schemmann, C. J. van der Poel, B. A. H. van Bakel, H. P. M. M. Ambrosius, A. Valster, J. A. M. van den Heijkant, and G. A. Acket, "Kink power in weakly index guided semiconductor lasers," *Appl. Phys. Lett.*, vol. 66, no. 8, pp. 920–922, Feb. 1995.

[9] J. Guthrie, G. L. Tan, M. Ohkubo, T. Fukushima, Y. Ikegami, T. Ijichi, M. Irikawa, R. S. Mand, and J. M. Xu, "Beam instability in 980-nm power lasers: Experiment and analysis," *IEEE Photon. Technol. Lett.*, vol. 6, no. 12, pp. 1409–1411, Dec. 1994.

[10] M. Ohkubo, Y. Ikegami, T. Ijichi, and T. Ninomiya, "Experimental study of beam steering in 980-nm InGaP cladding lasers," *Jpn. J. Appl. Phys.*, vol. 35, no. 1A, pp. L34–L36, Jan. 1996.

[11] W. D. Herzog, B. B. Goldberg, and M. S. Unlü, "Beam steering in narrow-stripe high-power 980-nm laser diodes," *IEEE Photon. Technol. Lett.*, vol. 12, no. 12, pp. 1604–1606, Dec. 2000.

[12] G. Hunziker and C. Harder, "Beam quality of InGaAs ridge lasers at high output power," *Appl. Opt.*, vol. 34, no. 27, pp. 6118–6122, Sep. 1995.

[13] J. W. R. ten Cate, L. M. Weegels, A. H. van Bakel, C. J. van der Poel, and H. P. M. Ambrosius, "Kinks induced by free-carrier absorption in weakly index guided semiconductor lasers," *Appl. Phys. Lett.*, vol. 71, no. 1, pp. 19–21, Jul. 1997.

[14] M. L. Xu, G. L. Tan, R. Clayton, and J. M. Xu, "Increased threshold for the first-order lateral mode lasing in low-ridge waveguide high power QW lasers," *IEEE Photon. Technol. Lett*, vol. 8, no. 11, pp. 1444–1446, Nov. 1996.

[15] G. L. Tan, R. S. Mand, and J. M. Xu, "Self-consistent modeling of beam instabilities in 980-nm fiber pump lasers," *IEEE J. Quantum Electron.*, vol. 33, no. 8, pp. 1384–1395, Aug. 1997.

[16] B. L. Frescura, C. J. Hwang, H. Luechinger, and J. E. Ripper, "Suppression of output nonlinearities in double-heterostructure lasers by use of misaligned mirrors," *Appl. Phys. Lett.*, vol. 31, no. 7, pp. 770–773, Dec. 1977.

[17] D. R. Scifres, W. Streifer, and R. D. Burnham, "GaAs/GaAlAs diode lasers with angled pumping stripes," *IEEE J. Quantum Electron.*, vol. QE-14, no. 4, pp. 223–227, Apr. 1978.

[18] A. D. Rakic, V. E. Boros, and M. L. Majewski, "Cooperatively frequency-locked multimode operation in proton implanted VCSELs," in *Proc. Conf. Optoelectron. Microelectron. Mater. Devices*, Perth, Australia, Dec. 14–16, 1998, pp. 116–119.

[19] H. Kogelnik, "Theory of optical waveguides," in *Guided-Wave Optoelectronics*, 2nd ed., T. Tamir, Ed. New York: Springer-Verlag, 1990, ch. 2.

[20] L. A. Coldren and S. W. Corzine, *Diode Lasers and Photonic Integrated Circuits*. New York: Wiley, 1995.

[21] J. W. Goodman, *Introduction to Fourier Optics*. New York: McGraw-Hill, 1968.

[22] M. Ito and T. Kimura, "Carrier density dependence of refractive index in AlGaAs semiconductor lasers," *IEEE J. Quantum Electron.*, vol. QE-16, no. 9, pp. 910–911, Sep. 1980.

Martin Achtenhagen received the Ph.D. degree in physics from the Swiss Federal Institute of Technology (EPFL), Lausanne, Switzerland, in 1996, for his work on gain-coupled distributed feedback (DFB) laser diodes.

After postdoctoral work at the IBM Zurich Research Laboratory, Zurich, Switzerland, he became a Research Staff Member at IBM Zurich in 1997 and was involved in work on quantum-well (QW) semiconductor lasers, with the emphasis on the design and characterization of high-power GaAs-based lasers. By ownership change, in 1997, he became a Research Staff Member of JDS Uniphase, Eatontown, NJ. In 1998, he was on leave for one year at Spectracom to develop a new generation of pump lasers for erbium-doped fiber amplifier (EDFA) applications and then returned to JDS Uniphase, where he managed the forward-looking group with emphasis on Raman amplifiers and EDFAs. In 2002, he became a Senior Research Associate at EPFL, Lausanne, Switzerland, where he is now working on the simulation of long-wavelength vertical-cavity surface-emitting laser diodes.

Dr. Achtenhagen serves as an Associate Editor of *Optical Fiber Technology*.

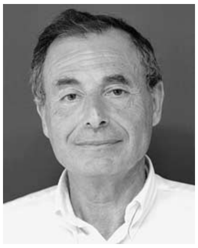

Amos A. Hardy (SM'84–F'97) received the B.Sc. and M.Sc. degrees in physics from the Hebrew University, Jerusalem, Israel, in 1966 and 1969, respectively and the Ph.D. degree in applied physics from the Weizmann Institute of Science, Rehovot, Israel, in 1975.

From 1975 to 1983, he was with the Department of Electronics, Weizmann Institute of Science. While at the Weizmann Institute, he held the Ruth E. Recu Career Development Chair. From 1976 to 1979, he was on leave at Stanford University, Stanford, CA, working on various laser resonator problems, optical phase conjugation, and optical rotation-sensing systems. During the summer of 1982, he was a Visiting Scientist at Bell Laboratories, Holmdel, NJ, where he worked on problems related to distributed feedback (DFB) lasers. Since 1983, he has been with the Faculty of Engineering at Tel Aviv University, Tel Aviv, Israel, where he was appointed as Associate Professor and later promoted to Professor in 1988. From June 1984 to July 1985, he was a Visiting Scientist at Xerox Palo Alto Research Center (PARC), Palo Alto, CA, where he was engaged in the analysis of phase-coupled laser arrays. During the summers of 1985 and 1986, he was a Visiting Associate Professor at the Center for High Technology Materials, University of New Mexico, Albuquerque. He was on sabbatical leave as a Senior Research Scientist at Spectra Diode Laboratories (SDL) during the academic year of 1988/1989 and spent several summers there until 2000. During these visits, he was engaged in the design and analysis of grating-coupled surface emitters, flared amplifiers, laser arrays, and fiber lasers and amplifiers. From 1991 to 1995, he served as Chairman of the Department of Electrical Engineering—Physical Electronics. In 1994 and 1995, and again in 2003 and 2006, he spent several months as Visiting Professor at Ecole Polytechnique Federale de Lausanne (EPFL), Switzerland, where he was engaged in DFB and vertical cavity lasers' theory. He is the incumbent Chana and Heinrich Manderman Chair in Optoelectronics. On several occasions, since 1997 until 2001, he was a Visiting Scientist at Uniphase Laser Enterprise (formerly IBM Laboratories), Zurich, Switzerland, where he was engaged in problems related to ridge lasers. During 2001 and 2002, he spent several months at Infinera, Sunnyvalle, CA, as a Research Scientist, developing models for optical amplifiers. His research interests involve analysis of dye laser systems, DFB lasers, distributed Bragg reflector (DBR) lasers, diode lasers, optical resonators and waveguides, fiber lasers and amplifiers, propagation of laser beams, optical phase conjugation, and the study of optical systems for inertial rotation sensing. He has performed research in several areas of lasers, integrated optics and electrooptics, optical phase conjugation, injection locking, grating analysis, resonator modes, beam propagation, coupled-mode theory, and other related fields. His work has been published in more than 180 refereed scientific papers and reported in many scientific meetings.

Dr. Hardy received, in 1993, the prize of the "Polish Jewish Ex-Servicemen Association—London" in the field of Applied Electronics for his contributions to the analysis and design of high-power coherent diode lasers. He is a Fellow of the Optical Society of America. He serves on the Editorial Board for the journal of *Microwave and Optical Technology Letters*.

Christoph S. Harder (M'82) received the Diploma EE degree from Swiss Federal Institute of Technology (ETH), Zurich, Switzerland, in 1979, and the Master EE and Ph.D. degrees from California Institute of Technology (Caltech), Pasadena, in 1980 and 1983, respectively.

He is Cofounder and Leader of the R&D effort of the IBM Zurich Laser Diode Enterprise, which pioneered the 980-nm high-power pump laser for telecom applications. Over the last few years, he and his research group expanded into the field of 14xx-nm telecom pumps, as well as 808- and 9xx-nm multimode pumps for industrial applications. He has held a variety of staff and management positions at Caltech, IBM, Uniphase, JDS Uniphase, Nortel, Bookham, and now ETH Zurich. He is the author or coauthor of more than 100 papers and is the holder of 20 patents.

Dr. Harder has served as General Chair at the International Semiconductor Laser Conference and at the LEOS Annual Meeting and on numerous technical and steering committees.